Progress In Electromagnetics Research, PIER 16, 153–173, 1997

WIDEBAND ELECTROMAGNETIC ANALYSIS OF FINITE-CONDUCTIVITY CYLINDERS

T. K. Sarkar

Electrical and Computer Engineering Department
Syracuse University, Syracuse, N.Y. 13244-1240, USA

A. R. Djordjević

School of Electrical Engineering
University of Belgrade, Yugoslavia

1. INTRODUCTION

We consider an array of M infinitely long cylindrical conductors of arbitrary cross sections (Figure 1). Each conductor is assumed to be made of a linear homogeneous nonmagnetic material of a finite conductivity $(\sigma_1, \ldots, \sigma_M)$. A time-harmonic regime is assumed, of an angular frequency ω. For each conductor the condition $\sigma \gg \omega\varepsilon_c$ is assumed to be fulfilled (where ε_c is the conductor permittivity), so that each conductor can be characterized by its complex permittivity $\varepsilon_e = -j\sigma/\omega$. The conductors are placed in a linear homogeneous dielectric, of parameters ε and μ. A cartesian coordinate system is

associated with the array, where the z-axis is parallel to the conductor axis. The array is assumed to be excited in such a way that there are only z-directed currents in the conductors, the density of which does not depend on z. This amounts to considering a two-dimensional system, with a magnetic field transverse to the z-axis (TM field).

The array under consideration can represent a model for various structures used in the engineering practice. Examples are a.c. power busses (where the proximity, edge and even skin effects can substantially affect conductor losses [Popović and Popović, 1972]), multiconductor transmission lines in communications and computers (where the model can be used to evaluate the frequency-dependent resistance and inductance matrices [Djordjević et al., 1985, Djordjević and Sarkar, 1986]), EMI/EMC shields in the form of screens or enclosures [Djordjević and Sarkar, 1991], as well as screens made of long parallel wires.

Two techniques for the analysis of the above array are presented and compared. The first technique is based on evaluating the current distribution within the conductors (it will be referred to as the volume-current formulation), and it has originally been used by power engineers, for low-frequency applications. The second technique is based on the concept of equivalent surface currents (and it will be referred to as the surface-current formulation), and it has been applied in various forms in solutions of high-frequency problems. These two techniques are presented in Sections 2 and 3, respectively. In Section 4 some specific aspects of applications of the two techniques to the analysis of transmission lines are elaborated. In Section 5 are given numerical examples which demonstrate some applications of the two methods and serve to compare these methods in various frequency ranges.

2. VOLUME-CURRENT FORMULATION

This technique has been applied in the solution of power-engineering problems of analyzing various buses [Popović and Popović, 1972]. It is based on formulating an integral equation for the distribution of the current within the conductor volume, and solving this equation using the method of moments [Harrington, 1993].

We assume that the excitation of the array of Figure 1 is modeled by an impressed (known) axial electric field ($\vec{E}_i = E_{iz}\hat{u}_z$, where $\hat{u}_z$ is the unit vector of the z-direction). This field can vary from one conductor to another, as well as across the cross section of a conductor, but it is assumed that there are no variations along the z-axis. In

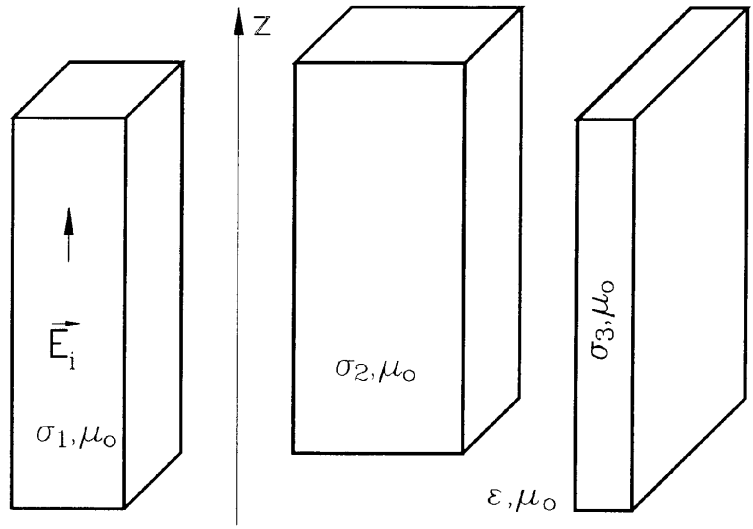

Figure 1. Sketch of an array of cylindrical conductors.

many practical cases this field is uniform over the cross section of each conductor, as shown in Section 4. As the response to this field, axial volume currents are induced in the conductors, and their density ($\vec{J} = J_z \hat{u}_z$) depends only on the transverse coordinates, and not on z (two-dimensional case). At each point of a conductor, the current density is related to the electric field by

$$\vec{J} = \sigma(\vec{E} + \vec{E}_i), \tag{1}$$

where $\vec{E}$ is the electric field produced by the conductor currents (and, generally, charges). This electric field can be expressed in terms of the magnetic vector-potential ($\vec{A}$) and the electric scalar-potential (V) as

$$\vec{E} = -j\omega\vec{A} - \text{grad}\, V. \tag{2}$$

The magnetic vector-potential is related to the currents, and the electric scalar-potential to the charges. The densities of the volume current ($\vec{J}$) and charges (ρ) are related by the continuity equation,

$$\text{div}\, \vec{J} = -j\omega\rho. \tag{3}$$

However, in our case $\partial J_z/\partial z = 0$, and $\rho = 0$. Hence, there can be no charges associated with our current, and $\text{grad}\, V = 0$, so that (2) reduces to

$$\vec{E} = -j\omega\vec{A}. \tag{4}$$

Assuming the medium to be nonmagnetic everywhere (i.e., $\mu = \mu_0$), and neglecting retardation in the dielectric in which the array of conductors is located (which is a valid assumption in power-engineering problems), the magnetic vector-potential is related to the currents, in the three-dimensional case, as

$$\vec{A} = \frac{\mu_0}{4\pi}\int_v \frac{\vec{J}dv}{r}, \tag{5}$$

where r is the distance between the source and the field points, and v is the volume in which the currents exist. Performing an integration over the z-coordinate results in the following expression for the magnetic vector-potential for the two-dimensional case

$$\vec{A} = -\frac{\mu_0}{2\pi}\int_S \vec{J}\log(r)dS, \tag{6}$$

where S denotes the cross section of all conductors, but this equation is subject to the condition that the total current of the array is zero,

$$\int_S \vec{J}\cdot d\vec{S} = 0. \tag{7}$$

Substituting (6) into (4), and (4) into (1) results in an integral equation for the volume-current density $\vec{J}$,

$$-j\omega\frac{\mu_0}{2\pi}\int_S \vec{J}\log(r)dS + \frac{\vec{J}}{\sigma} = \vec{E}_i, \tag{8}$$

which is valid for any point within any conductor of the array. Both sides of equation (8) should be projected on the z-axis, reducing to

$$-j\omega\frac{\mu_0}{2\pi}\int_S J_z(x',y')\log(r)dx'dy' + \frac{J_z(x,y)}{\sigma} = E_{iz}(x,y), \tag{9}$$

which is an integral equation for $J_z(x,y)$, where x and y are transverse coordinates. For convenience, the coordinates of the source point are denoted by primes, so that $r = \sqrt{(x-x')^2 + (y-y')^2}$.

Equation (9) can be solved numerically, using the method of moments [Harrington, 1993]. We adopt here the pulse approximation for the current distribution, which is the simplest choice. (More sophisticated approximations can involve entire-domain expansion functions, or even inclusion of skin-effect terms.) To that purpose, we divide the cross section of each conductor in a number of rectangular cells, and assume the current to be uniformly distributed over each cell. This amounts to defining a set of expansion functions,

$$f_i(x,y) = \begin{cases} 1 & \text{on rectangle } \#i \\ 0 & \text{elsewhere} \end{cases}, \tag{10}$$

and taking

$$J_z(x,y) = \sum_{i=1}^{n} J_i f_i(x,y), \tag{11}$$

where n is the total number of rectangles, and J_i are constants to be solved for. When (11) is substituted into (9), we obtain

$$-j\omega\frac{\mu_0}{2\pi}\sum_{i=1}^{n} J_i \int_{S_i} \log(r)dx'dy' + \frac{1}{\sigma_j}J_j = E_{izj}, \quad j = 1,\ldots,n, \tag{12}$$

where S_i denotes the surface of the rectangle $\#\,i$, and σ_i the conductivity at that rectangle. The simplest choice of weighting functions are impulses, which amounts to the point-matching method, which we adopt here. The matching points are chosen at centroids of the n rectangles. The resulting integrals in equation (12) can be solved analytically, as given in Appendix. After the system of linear equations in J_i is solved, the total current of each conductor can be evaluated as

$$I_m = \sum_i J_i S_i, \tag{13}$$

where the summation is taken over all pulses for that conductor.

The impressed electric field in the above equations cannot be arbitrarily specified for all conductors, because the condition (7) must hold. One way to bypass this problem is to subtract the last point-matching equation from all the previous equations (in a similar way as in [Djordjević et al., 1989]), and replace the last equation by

$$\sum_{i=1}^{n} J_i S_i = 0. \tag{14}$$

Another possibility for achieving the same goal is presented in Section 4.

3. SURFACE-CURRENT FORMULATION

The basic idea of this method is to use equivalence theorems [Harrington, 1961] to break the system under considerations into a number of subsystems, each of them being filled with a homogeneous medium. In this formulation we can include ferromagnetic properties of conductors by taking conductor permittivities to be $\mu_1, \ldots, \mu_M$.

Illustrated in Figure 2 is the basic application of the equivalence theorems. Shown in Figure 2a is the cross section of the conductor array of Figure 1. Figure 2b shows the equivalent system for the exterior region (the dielectric in which the conductors are embedded), and Figure 2c shown the equivalent system for the interior region of one conductor. (Similar systems should be simultaneously observed for all other conductors.) In each of the equivalent systems, a layer of surface electric currents (of density $\vec{J}_s$), and a layer of surface magnetic currents (of density $\vec{M}_s$) are placed on the surfaces of discontinuity (conductor surfaces), with the objective to produce a zero total field in a region. The medium in the region with a zero field can be replaced by any other medium, which enables us to imagine that the medium in an equivalent system is homogeneous everywhere. The homogenization of the medium is necessary for using the simplest form of Green's functions for the potentials, as given below.

In order to achieve the equivalence in Figure 2, the densities of the equivalent surface currents must obey the following relations

$$\vec{J}_s = \hat{n} \times \vec{H}, \tag{15}$$

$$\vec{M}_s = -\hat{n} \times \vec{E}, \tag{16}$$

where $\vec{E}$ and $\vec{H}$ are the fields at the surface which existed there before the substitution, and $\hat{n}$ is the unit normal on the interface directed towards the region with nonzero field. The surface currents in the systems of Figures 2b and 2c are equal in magnitude, but opposite in direction.

The electric and magnetic fields can be expressed in terms of the potentials as

$$\vec{E} = -j\omega\vec{A} - \frac{1}{\varepsilon}\text{curl}\,\vec{F} + \vec{E}_i, \tag{17}$$

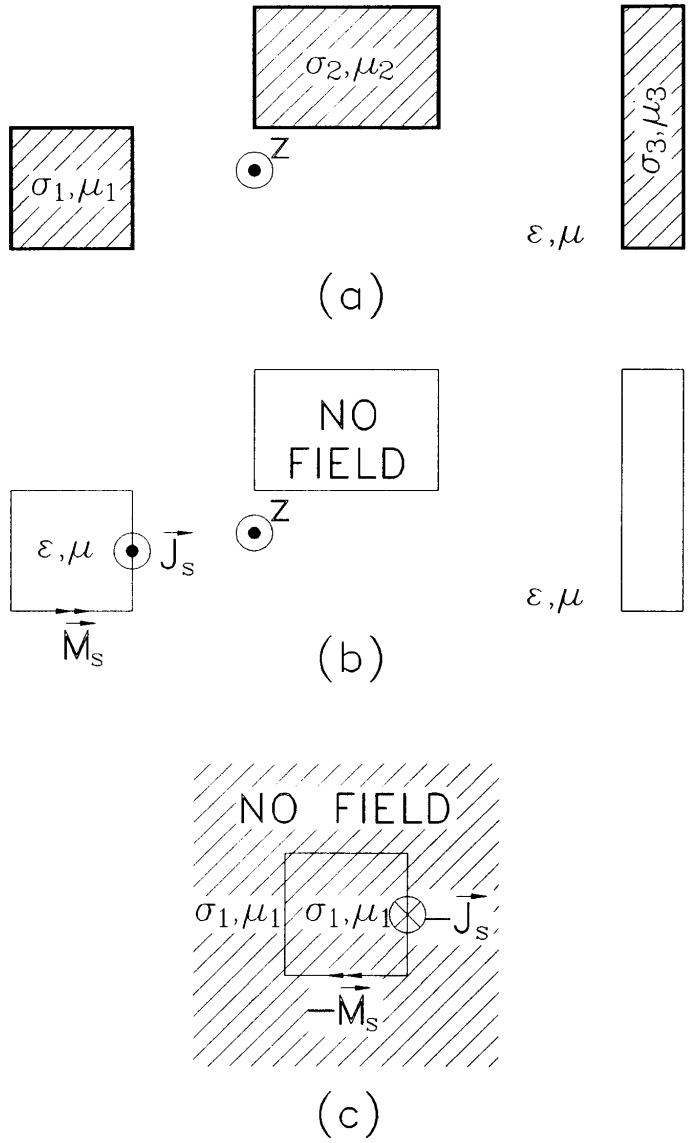

Figure 2. (a) Cross section of the array of Figure 1, and the equivalent systems for (b) the exterior region, and (c) interior region of conductor #1.

$$\vec{H} = -j\omega\vec{F} - \text{grad}\, V_m + \frac{1}{\mu}\text{curl}\, \vec{A} + \vec{H}_i, \tag{18}$$

where $\vec{F}$ is the electric vector-potential, V_m the magnetic scalar-potential, and $\vec{E}_i$ and $\vec{H}_i$ describe the excitation. (The $\text{grad}\, V$ term is missing in (17) because we again assume the electric currents to be z-directed, with no z-variation.) The potentials in these expressions are given by

$$\vec{A} = \mu \int_s \vec{J}_s g(r) ds, \tag{19}$$

$$\vec{F} = \varepsilon \int_s \vec{M}_s g(r) ds, \tag{20}$$

$$V_m = \frac{1}{\mu} \int_s \rho_{ms} g(r) ds, \tag{21}$$

where s is the circumference of the boundary surfaces where the equivalent currents are located. The exact Green's function (for the two-dimensional case) for the exterior region is

$$g(r) = -\frac{j}{4} H_0^{(2)}(kr), \tag{22}$$

where $H_0^{(2)}$ is Hankel's function of the second kind and order zero, and $k = \omega\sqrt{\varepsilon\mu}$ is the phase coefficient, and it includes the retardation. This function is proportional to the potential produced by an infinite, uniform line source and it is obtained by integrating $\exp(-jkr)/(4\pi r)$ over z, from $-\infty$ to $+\infty$. In the limiting quasi-static case Green's function (22) tends to $-\frac{1}{2\pi}\log(kr)$, thus yielding the kernel of equation (6).

For the interior region we have

$$g(r) = \frac{1}{2\pi}[ker(|\gamma|r) + j\, kei(|\gamma|r)], \tag{23}$$

where ker and kei are Kelvin's functions, and $\gamma = \sqrt{j\omega\mu\sigma}$ is the propagation coefficient in the conductor.

In order to have a zero field within a region in an equivalent system of Figure 2, according to equivalence theorems it is sufficient to impose the condition than the tangential component of either the electric

field, or the magnetic field vanishes at the boundary surface. (Exceptional situations are internal resonances of bounded regions, which may be a problem in the system of Figure 2b only if the cross section of a conductor is of the order of the wavelength.) Imposing the first condition leads to the electric-field integral equation (EFIE) for the equivalent surface currents, and imposing the second conditions leads to the magnetic-field integral equation (MFIE). Our extensive numerical experiments have shown that the choice of EFIE for the system of Figure 2b, i.e., imposing

$$\vec{E}_{\text{tang}} = 0 \tag{24}$$

at the interfaces, and MFIE for the system of Figure 2c, i.e., imposing

$$\vec{H}_{\text{tang}} = 0, \tag{25}$$

provides the widest frequency range in which the present method can be applied [Djordjević et al., 1985].

In order to avoid a confusion about the impressed electric and magnetic fields, our recommendation is not to specify the impressed fields, but rather sources of this field. Such an approach yields both the impressed electric and magnetic fields, which is important in cases when both of them are needed (such as in combined-field integral equations). For example, if we analyze a transmission line (see Section 4), the sources of the impressed fields can be solenoidal sheets of transverse magnetic currents, wrapping each conductor (including the equivalent surface currents). Such a solenoid practically produces a uniform impressed electric field within a conductor in the system of Figure 2b. However, in the system of Figure 2c there is no impressed field, because the solenoid is located in the exterior region.

The approximate solution of these coupled integral equation is obtained using the simplest combination of pulse expansion functions and point-matching. Line magnetic charges are associated with this approximation of the magnetic currents. (More sophisticated expansions can also be used, e.g., a continuous expansion for the magnetic currents, which results in no line magnetic charges.) The matching points are located at the subsection midpoints. For the system of Figure 2b, the matching points are located at the inner side of the boundary surfaces, and for the system of Figure 2c, the matching points are located at the outer side. Taking into account

$$\text{grad}\, g(r) = \frac{dg}{dr}\hat{u}_r, \tag{26}$$

where $\hat{u}_r$ is the unit vector in the radial direction, for the exterior problem we have

$$-j\omega\vec{A} = -j\zeta\vec{J}_s \int_s \left(-\frac{j}{4}\right) H_0^{(2)}(kr)d(ks), \tag{27}$$

$$-\frac{1}{\varepsilon}\text{curl}\,\vec{F} = \vec{M}_s \times \int_s \frac{j}{4} H_0^{(2)}(kr)\hat{u}_r d(ks), \tag{28}$$

where $\zeta = \sqrt{\mu/\varepsilon}$ is the wave impedance of the dielectric, while for the interior problem we have

$$-j\omega\vec{F} = -\frac{\vec{M}_s}{|\hat{\zeta}|} \int_s \frac{1}{2\pi}[ker(|\gamma|r) + j\, kei(|\gamma|r)]d(|\gamma|s), \tag{29}$$

$$-\frac{1}{\varepsilon}\text{curl}\,\vec{A} = -\vec{J}_s \times \int_s \frac{1}{2\pi}[ker'(|\gamma|r) + j\, kei'(|\gamma|r)]\hat{u}_r d(|\gamma|s), \tag{30}$$

$$-\text{grad}\,V_m = -|\vec{M}_s| \left[\frac{j}{2\pi|\hat{\zeta}|}[ker'(|\gamma|r) + j\, kei'(|\gamma|r)\hat{u}_r\right]_{r=r_1}^{r_2}, \tag{31}$$

where r_1 and r_2 are distances between the end points of a pulse and the field point, and $\hat{\zeta} = \sqrt{j\omega\mu/\sigma}$ is the wave impedance of the conductor. Equations (29)–(31) yield a natural condition at higher frequencies

$$\vec{M}_s = \hat{\zeta}\hat{n} \times \vec{J}_s, \tag{32}$$

where $\hat{\zeta}$ is the wave impedance of the conductor, and $\hat{n}$ the outer normal.

4. APPLICATION TO ANALYSIS OF MULTICONDUCTOR TRANSMISSION LINES

In the quasi-static analysis of transmission lines, the evaluation of matrices $[B']$ (matrix of electrostatic-induction coefficients per unit length, or the capacitance matrix) and $[G']$ (matrix of conductances per unit length) is carried out independently from the analysis of the matrices $[L']$ (matrix of inductances per unit length) and $[R']$ (matrix of resistances per unit length) [Djordjević et al., 1989]. In many cases, the results are required only for high frequencies, when the skin effect is fully developed. In those cases, the matrix $[L']$ is computed by inverting the matrix $[B'_0]$, which is evaluated when the transmission line

dielectrics are replaced by vacuum, and the matrix $[R']$ is thereby evaluated by perturbation method. The resulting matrix $[L']$ is frequency independent, while the matrix $[R']$ is proportional to $\sqrt{f}$ where f is the operating frequency. At the low-frequency end (towards the d.c. case), however, the current becomes uniformly distributed over a conductor cross section, there exist effects of the internal inductance, and the resistance tends to the d.c. value. In the intermediate region between the low and high frequencies, the edge and proximity effects take part in addition to the skin effect, which altogether leads to complicated variations of the matrices $[L']$ and $[R']$ versus frequency [Djordjević and Sarkar, 1993]. The two techniques presented in this paper can be used to evaluate these variations in a broad frequency range. Thereby, the volume-current formulation is more convenient for low frequencies, but it breaks down going into skin-effect region, as will be demonstrated in Section 5. The surface-current formulation is more convenient for medium and high frequencies. For both techniques, some remarks should be given about the impressed electric field and the evaluation of the matrices $[L']$ and $[R']$.

For a real transmission line, the sources of the electric field are currents and charges. Assuming a pure TEM wave, the currents are axial, and so are the magnetic vector-potential and the electric field produced by these currents. The charges produce two components of the electric field: the transverse one (which gives rise to the voltage between the conductors) and the axial one (which is fully annihilated with the electric field produced by the currents). It is well-known from the transmission-line theory that the electric field within one cross section of a transmission line has the same pattern as in the electrostatic case. As a consequence, a (perfect) conductor is equipotential, i.e., the electric scalar-potential V (which is produced by the charges) is constant over the cross section of a conductor. Thus for the case of Figure 3 we have $V_1 = V_4$ and $V_2 = V_3$. Since

$$\oint_C \operatorname{grad} V \cdot d\vec{l} = 0 \tag{33}$$

for an arbitrary closed path, for the rectangular path 1-2-3-4-1 in Figure 3 we have $\oint_C \operatorname{grad} V \cdot d\vec{l} = (V_2 - V_1) + (V_3 - V_2) + (V_4 - V_3) + (V_1 - V_4) = (V_2 - V_1) - (V_3 - V_4) = 0$. If we assume assume that the distance Δz between the points 1 and 2 (or 4 and 3) is small, then $\hat{u}_z \cdot \operatorname{grad} V \approx (V_2 - V_1)/\Delta z$ along 1-2, and $\hat{u}_z \cdot \operatorname{grad} V \approx (V_3 - V_4)/\Delta z$

along 4-3. It is hence obvious that the axial component of grad V is uniform over the conductor cross section.

In our two-dimensional model of the array of conductors, only the axial component of the electric field is relevant. The component $-\hat{u}_z \cdot \text{grad}\, V$ must appear in equations, although there is no charge in our model to produce it. It is the impressed electric field that actually replaces the axial field produced by the charges, and this field is uniform within a conductor.

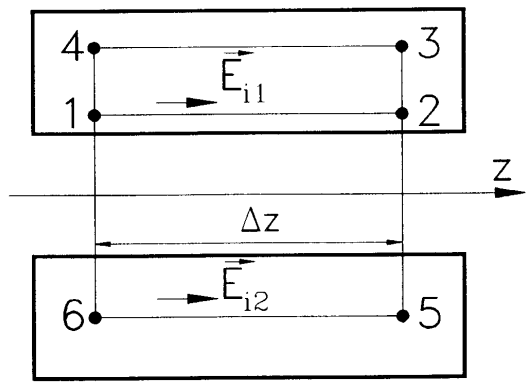

Figure 3. Sketch of a transmission line with two conductors.

The circulation of grad V is also zero for the rectangular path 1-2-5-6-1 in Figure 3. Since $V_1 - V_6$ is the transmission-line voltage at the first cross section, and $V_2 - V_5$ at the second cross section, it is obvious that $-\hat{u}_z \cdot \text{grad}\, V$ is responsible for the voltage drop along the transmission line. This component being replaced by the impressed electric field, the voltage drop per unit length along the line is now

$$\frac{dV}{dz} = -(E_{i1z} - E_{i2z}). \tag{34}$$

From telegraphers' equations we have

$$\frac{dV}{dz} = -Z'I, \tag{35}$$

where $Z' = R' + j\omega L'$ is the impedance per unit length of the line, R' is the resistance per unit length, and L' the inductance per unit length.

Let us consider a transmission line with $M = N + 1$ conductors ($M \geq 2$). The impressed fields must not be arbitrarily specified for all M conductors, because the condition (7) would be violated in the general case. Note that (7) must be fulfilled not only for equation (6) to be valid, but also to properly model a multiconductor transmission line, because equation (7) is valid for a TEM wave (and practically for a quasi-TEM wave), i.e.,

$$\sum_{m=1}^{M} I_m = 0, \tag{36}$$

where I_m is the current of conductor $\# m$ with respect to the reference direction of the z-axis. In the analysis of multiconductor transmission lines [Djordjević et al., 1987], usually one conductor (say, $\# M$) is assumed to be the reference conductor ("ground"), and the voltages between the other, signal conductors and the reference conductor, $V_{1M}, \ldots, V_{NM}$, are used to describe the state on the line. From equation (34) it follows that

$$\frac{dV_{mM}}{dz} = E_{iMz} - E_{imz}. \tag{37}$$

A generalization of (35) yields

$$\frac{d[V]}{dz} = -[Z'][I], \tag{38}$$

where

$$[V] = [V_{1M}, \ldots, V_{NM}]^t \tag{39}$$

is the column-matrix of voltages between the signal conductors and the reference conductor ("t" denotes transpose),

$$[I] = [I_1, \ldots, I_N]^t \tag{40}$$

is the column-matrix of the signal-conductor currents, and $[Z']$ is a square (N by N) matrix of impedances per unit length,

$$[Z'] = [R'] + j\omega[L']. \tag{41}$$

For a transmission line we can specify dV_{mM}/dz arbitrarily, but we have to force (7) or (36) to be valid. One way to achieve this goal is the

following procedure [Djordjević and Sarkar, 1986]. We introduce the augmented vector of current intensities (which includes all $M = N+1$ conductors),

$$[I^a] = [I_1, \ldots, I_M]^t, \tag{42}$$

and the vector of impressed electric fields,

$$[E_i] = [E_{i1z}, \ldots, E_{iMz}]^t. \tag{43}$$

The following equation is valid because the system is linear

$$[I^a] = [T][E_i], \tag{44}$$

where $[T]$ is a square (M by M) matrix. The element T_{mn} numerically equals the current I_m when $E_{inz} = 1\,\mathrm{V/m}$, and all the other impressed fields are zero. We now take $n = 1, \ldots, M$ and evaluate the elements of the matrix $[T]$. Note that this procedure has no physical interpretation if the volume-current formulation is used, because each time the currents are evaluated, equation (7) is violated. Furthermore, if the units for coordinates are changed, different answers for the currents will be obtained. However, this numerical procedure yields correct final results for the matrix $[Z']$. From (44) we have

$$[E_i] = [Z^{a\prime}][I^a], \tag{45}$$

where

$$[Z^{a\prime}] = [T]^{-1} \tag{46}$$

is the augmented matrix of impedances per unit length. Equivalently,

$$E_{imz} = \sum_{m=1}^{M} {Z^{a\prime}}_{mn} I_n. \tag{47}$$

From (36) we have

$$I_M = -\sum_{m=1}^{N} I_m, \tag{48}$$

so that

$$E_{imz} - E_{iMz} = \sum_{n=1}^{N} \left[{Z^{a\prime}}_{mn} - {Z^{a\prime}}_{mM} - {Z^{a\prime}}_{Mn} + {Z^{a\prime}}_{MM} \right] I_n, \qquad m = 1, \ldots, N, \tag{49}$$

and the elements of the matrix $[Z']$ are evaluated as

$$Z'_{mn} = Z^{a\prime}{}_{mn} - Z^{a\prime}{}_{mM} - Z^{a\prime}{}_{Mn} + Z^{a\prime}{}_{MM}, \quad m, n = 1, \ldots, N. \tag{50}$$

5. EXAMPLES

The first example is the microstrip line, sketched in Figure 4. The width of the signal conductor is $w = 0.2\,\text{mm}$, the substrate thickness is $h = 0.1\,\text{mm}$, the ground plane width is finite, $g = 2\,\text{mm}$, and the thickness of the signal conductor and the ground plane is $t = 0.01\,\text{mm}$. The conductors are assumed to be made of copper, of conductivity $\sigma = 56\,\text{MS/m}$. Shown in Figure 5 are the resistance per unit length and the inductance per unit length of this line, obtained by the two techniques presented in this paper. For the first technique the conductors were uniformly divided into pulses (rectangles): $n_w = 10$ along w, $n_g = 40$ along g and $n_t = 3$ along t, resulting in the total of 150 unknowns. For the second technique the contours of the conductors were nonuniformly segmented (segment widths progressively smaller going towards the wedges) into $n_w = 25$, $n_g = 50$ and $n_t = 3$ pulses, respectively, resulting in a total of 324 unknowns (for electric and magnetic currents).

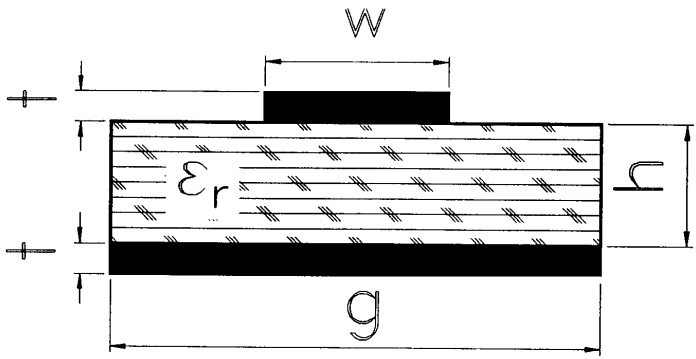

Figure 4. Sketch of a microstrip line.

Figure 5 illustrates some features of the two techniques. The volume -current formulation yields excellent results at low frequencies. For example, for $f = 10\,\text{kHz}$, the numerical results are $L' = 440.5\,\text{nH/m}$

and $R' = 9.821\,\Omega/\mathrm{m}$, while the analytically calculated values [Djordjević and Sarkar, 1993] are $L' = 439.27\,\mathrm{nH/m}$ and $R' = 9.821\,\Omega/\mathrm{m}$. The surface-current formulation yields a smaller accuracy, especially as the frequency becomes very low, primarily due to the $-\mathrm{grad}\,V$ term in equation (18). The accuracy can be improved at the expense of taking more pulses. In the medium-frequency region (300 kHz–30 MHz) the agreement between the two techniques is excellent. In the high-frequency (skin-effect) region the results for R' obtained by the volume-current formulation saturate, instead of increasing as $\sqrt{f}$. This is due to the pulse approximation for the current distribution, as there must always be a current in the outermost layer of pulses, while actually the thickness of the current layer constantly decreases with increasing the frequency. The results for R' obtained by the surface-current formulation follow very well the $\sqrt{f}$ behavior. However, at very high frequencies (above about 10 GHz) R' starts increasing much faster. This is a consequence of radiation. Namely, the structure behaves like a two-dimensional magnetic dipole, the radiation resistance of which is proportional to f^3 [Djordjević et al., 1985]. The radiation is a consequence of a uniform current distribution in the z-direction and will not occur on a real transmission line if the phase velocity of the current is identical to that in the surrounding dielectric medium $(1/\sqrt{\varepsilon\mu})$. However, if a deviation occurs (e.g., due to discontinuities or a hybrid nature of the wave caused by inhomogeneous dielectrics), radiation will take place, but it will be pronounced at somewhat higher frequencies than indicated by Figure 5. There would be no radiation effects in the numerical model if the quasi-static kernel of equation (6) were used instead of (22).

The second example are two coupled microstrip lines, sketched in Figure 6, of dimensions $w = 0.6\,\mathrm{mm}$, $s = 0.02\,\mathrm{mm}$, $g = 2\,\mathrm{mm}$, $h = 0.1\,\mathrm{mm}$, $t = 0.02\,\mathrm{mm}$, and the conductors are assumed to be made of copper. Given in Table 1 are the elements of the matrices $[R']$ and $[L']$ for several frequencies, as computed by the two techniques. Large changes in the element values can be observed, including a change in sign of the mutual terms. For comparison, the exact d.c. values for the elements of the matrix $[R']$ are $R'_{11} = R'_{22} = 1.935\,\Omega/\mathrm{m}$ and $R'_{12} = R'_{21} = 0.446\,\Omega/\mathrm{m}$, while the electrostatic analysis [Djordjević et al., 1989] yields the high-frequency values (at $f = 1\,\mathrm{GHz}$) $L'_{11} = L'_{22} = 128.2\,\mathrm{nH/m}$, $L'_{12} = L'_{21} = 36.6\,\mathrm{nH/m}$, $R'_{11} = R'_{22} = 23.47\,\Omega/\mathrm{m}$, $R'_{12} = R'_{21} = -2.53\,\Omega/\mathrm{m}$.

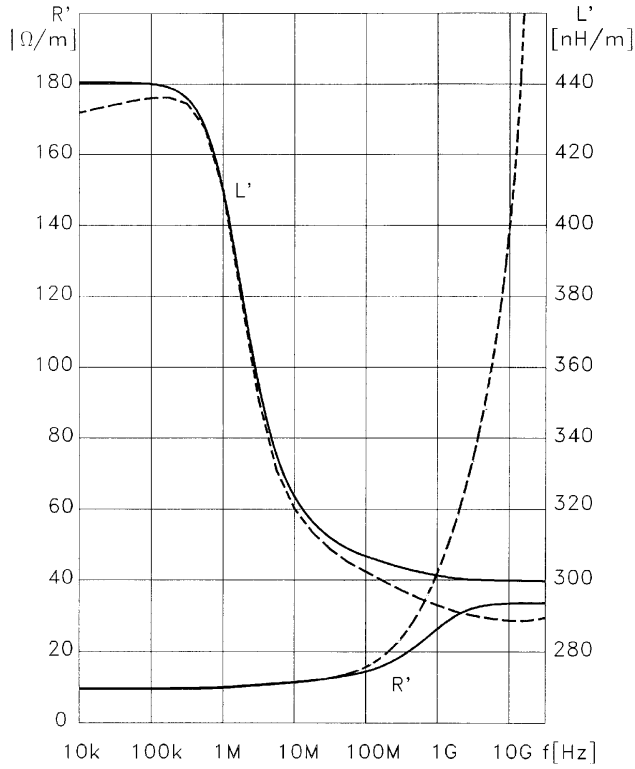

Figure 5. Resistance per unit length (R') and inductance per unit length (L') of the microstrip line of Figure 4, versus frequency (f), computed using the volume-current formulation (——) and the surface-current formulation (— —).

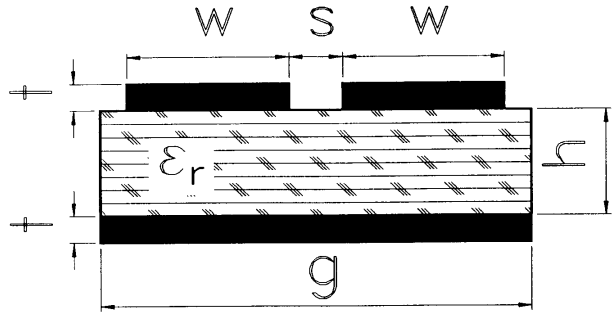

Figure 6. Sketch of two coupled microstrip line.

f [Hz]	Volume-current formulation				Surface-current formulation			
	$L'_{11}=L'_{22}$ [nH/m]	$L'_{12}=L'_{21}$ [nH/m]	$R'_{11}=R'_{22}$ [Ω/m]	$R'_{12}=R'_{21}$ [Ω/m]	$L'_{11}=L'_{22}$ [nH/m]	$L'_{12}=L'_{21}$ [nH/m]	$R'_{11}=R'_{22}$ [Ω/m]	$R'_{12}=R'_{21}$ [Ω/m]
10 k	253.9	-26.4	1.935	0.446	247.8	-24.3	1.898	0.459
100 k	250.7	-23.9	1.945	0.440	247.9	-23.1	1.908	0.451
1 M	187.1	15.6	2.183	0.316	184.8	16.5	2.149	0.327
10 M	156.2	30.2	2.576	0.161	152.8	11.9	2.694	0.075
100 M	149.1	29.9	4.653	0.912	139.7	35.4	6.829	-0.263
1 G	146.0	29.0	7.576	1.437	131.9	36.1	23.28	-2.25
10 G	145.9	29.0	7.748	1.457	122.9	36.4	77.19	-1.80

Table 1. Matrix elements of coupled microstrip lines sketched in Figure 6.

6. CONCLUSION

Two methods for analysis of arrays of infinitely long, parallel conductors were presented and compared. The first method, referred to as the volume-current formulation, is simpler for implementation. It can be useful not only for power-engineering problems, but also for thin and thick-film structures, even in the gigahertz region, because of the small conductor dimensions. The practical upper limit for the technique is a few times the frequency at which the conductor thickness becomes equal to the skin depth. This technique can efficiently be combined with the perturbation approach, which is valid in the skin-effect region, to cover the full frequency range.

The second technique, referred to as the the surface-current formulation, can be used to cover the full frequency range, but with a caution for very low frequencies. It includes radiation effects, and gives excellent results in the medium and high-frequency regions. The technique can be extended to the analysis of systems with piecewise-homogeneous dielectrics, even to perform a full-wave analysis of guiding structures [Olyslager et al., 1993] or to evaluate shielding effectiveness taking into account both field penetration through the metallic shield, as well as slots in the shield [Djordjević and Sarkar, 1991].

ACKNOWLEDGEMENT

This work was supported in part by E. I. Dupont de Nemours and Company and by the CASE Center of Syracuse University.

REFERENCES

1. Djordjević, A. R., T. K. Sarkar, and S. M. Rao, "Analysis of finite conductivity cylindrical conductors excited by axially-independent TM electromagnetic field", *IEEE Trans. on Microwave Theory and Techniques*, Vol. MTT-33, No. 10, 960–966, October 1985.
2. Djordjević, A. R., and T. K. Sarkar, "Frequency behaviour of multiconductor transmission line inductances and resistances", *Archiv für Elektronik und Übertragungstechnik*, B. 40, H. 4, 254–256, April 1986.
3. Djordjević, A. R., T. K. Sarkar, and R. F. Harrington, "Time-domain response of multiconductor transmission lines", *Proc. IEEE*, Vol. 75, No. 6, 743–764, June 1987.
4. Djordjević, A. R., R. F. Harrington, T. K. Sarkar, and M. B. Bazdar, *Matrix Parameters for Multiconductor Transmission Lines (Software and User's Manual)*, Boston: Artech House, 1989.
5. Djordjević, A. R., and T. K. Sarkar, "Evaluation of shielding effectiveness of cylindrical metallic shields", *Proc. of 9th Int. Zurich Symp. on Electromagnetic Compatibility*, Zurich, March 1991.
6. Djordjević, A. R., and T. K. Sarkar, "Closed-form formulae for frequency-dependent resistance and inductance per unit length of microstrip and strip transmission lines", in print in *IEEE Trans. on Microwave Theory and Techniques*, 1993.
7. Harrington, R. F., *Time-Harmonic Electromagnetic Fields*, New York: McGraw-Hill, 1961.
8. Harrington, R. F., *Field Computation by Moment Methods*, New York: IEEE Press, 1993.
9. Olyslager, F., D. DeZutter, and K. Blomme, "Rigorous analysis of the propagation characteristics of general lossless and lossy multiconductor transmission lines in multilayered media", *IEEE Trans. on Microwave Theory and Techniques*, Vol. MTT-41, No. 1, 79–88, January 1993.
10. Popović, B. D., and Z. D. Popović, "Method for determining power frequency current distribution in cylindrical conductors", *Proc. IEE*, Vol. 119, No. 5, 569–574, May 1972.

APPENDIX. EVALUATION OF THE INTEGRAL IN EQUATION (9)

Consider a rectangular cell (Figure 7) carrying a uniform current. The integral in equation (12) for this cell (S_i) has the form

$$K(a,b,x,y) = -\int_{-b/2}^{b/2}\int_{-a/2}^{a/2} \log\sqrt{(x-x')^2+(y-y')^2}dx'dy'. \quad (51)$$

We can use the complex calculus, and set $z_1 = x' + j0$ and $z_2 = 0 + iy'$. The inner integration in the complex plane is along the real axis, so that $dx' = dz_1$, and the outer integration is along the imaginary axis, so that $dy' = -jdz_2$. We can also set $z = x + jy$, which maps the matching point to a point in the complex plane. Now,

$$\log\sqrt{(x-x')^2+(y-y')^2} = \mathrm{Re}\{\log(z - z_1 - z_2)\}, \quad (52)$$

since

$$\log(z) = \log|z| + j\arg(z). \quad (53)$$

Note that $\log(z)$ has a branch cut, which causes problems. On most computers $-\pi < \arg(z) \leq \pi$, and the branch cut is along the negative part of the real axis. We define

$$K_2(z) = \iint \log(z)dz = \frac{z^2}{2}\left[\log(z) - \frac{3}{2}\right], \quad (54)$$

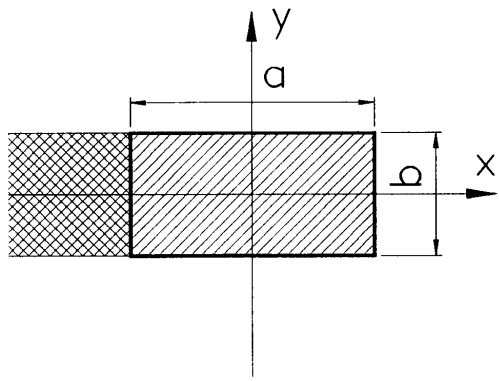

Figure 7. Coordinate system for evaluation of the integral in Equation (7).

where the subscript "2" denotes a double integral. Note that $K_2(0) = 0$. Hence, the double integral in equation (51) can be evaluated as

$$K(a,b,x,y) = \mathrm{Re}\left\{ jK_2(z - z_1 - z_2)\Big|_{z_1=-a/2}^{a/2}\Big|_{z_2=-jb/2}^{jb/2} \right\}. \qquad (55)$$

However, this result is valid only outside the hatched regions of Figure 7. When the point z horizontal boundary of a hatched region, the argument of one or two logarithms in equation (55) abruptly changes for 2π due to the branch cut, which causes an error in the result. This error can be compensated by adding the term $-\pi(a-x)^2$ to K if the point is in the single-hatched area, and by adding $\pi[(a+x)^2-(a-x)^2]$ if the point is in the double-hatched area.